

1 **Supplementary Information for**
2 **Evaluating Simulations of Organic Aerosol Volatility and Degree of Oxygenation**
3 **in Eastern China**

4 Yu Li¹, Momei Qin^{1*}, Weiwei Hu², Bin Zhao³, Ying Li⁴, Hava O. T. Pye⁵, Jingyi Li¹, Linghan
5 Zeng⁶, Song Guo⁷, Min Hu⁷, Jianlin Hu¹

6 ¹ Jiangsu Key Laboratory of Atmospheric Environment Monitoring and Pollution Control, Col-
7 laborative Innovation Center of Atmospheric Environment and Equipment Technology, School
8 of Environmental Science and Engineering, Nanjing University of Information Science and
9 Technology, Nanjing 210044, China

10 ² State Key Laboratory of Organic Geochemistry, Guangzhou Institute of Geochemistry, Chi-
11 nese Academy of Sciences, Guangzhou 510640, China

12 ³ State Key Laboratory of Regional Environment and Sustainability, School of Environment,
13 Tsinghua University, Beijing 100084 China

14 ⁴ School of Environmental Science and Technology, Dalian University of Technology, Dalian
15 116024, China

16 ⁵ Gillings School of Global Public Health, University of North Carolina at Chapel Hill, Chapel
17 Hill, North Carolina 27599, United States

18 ⁶ State Key Laboratory of Atmospheric Environment and Extreme Meteorology, Institute of
19 Atmospheric Physics, Chinese Academy of Sciences, Beijing 100029, China

20 ⁷ State Key Laboratory of Regional Environment and Sustainability, International Joint Labor-
21 atory for Regional Pollution Control, Ministry of Education (IJRC), College of Environmental
22 Sciences and Engineering, Peking University, Beijing 100871, China

23

24 *Corresponding author: Momei Qin (momei.qin@nuist.edu.cn)

25 **This PDF file includes:**

26 Supplementary Notes 1-2

27 Supplementary Tables S1-S10

28 Supplementary Figures S1-S19

29 Supplementary References

30

31 Supplementary Notes 1: Estimation of L/S/IVOC Emissions

The L/S/IVOC emission inventory was developed based on VOC and POA emissions from MEICv1.4, considering the strong correlation between IVOC and VOC emissions and similar definitions of POA and S/LVOCs. In MEICv1.4, emissions are classified into five major source categories (power plants, industry, residential, transportation, and agriculture) and further divided into 22 subcategories. IVOC emissions for each subcategory were estimated using source-specific scaling factors ($f_{IVOC,i,j}$) applied to total VOC emissions, as expressed in Equation S1. S/LVOC emissions resulted from the semi-volatile fraction of POA were estimated using the corresponding scaling factor ($f_{S/LVOC,i,j}$) relative to POA, as shown in Equation S2. IVOC and S/LVOC emissions were then distributed into four volatility bins: $10^3 \mu\text{g m}^{-3}$ to $10^6 \mu\text{g m}^{-3}$ for IVOCs and $10^{-2} \mu\text{g m}^{-3}$ to $10^2 \mu\text{g m}^{-3}$ for S/LVOCs, with an interval of one order of magnitude per bin. The equations are as follows:

$$E_{IVOC,i,j} = E_{VOC,i,j} * f_{IVOC,i,j} \quad (S1)$$

$$E_{SLVOC,i,j} = E_{POA,i,j} * f_{S/LVOC,i,j} \quad (S2)$$

45 Here, i represents the emission source category, j denotes the volatility bin, and $E_{IVOC,i,j}$ and
 46 $E_{SLVOC,i,j}$ are the estimated IVOC and S/LVOC emissions (in tons) for each source i and bin j .
 47 The scaling factors f were obtained from the literature, with more details provided in Table S3.

49 Supplementary Notes 2: Calculation of glass transition temperature (T_g) and viscosity

50 The glass transition temperature of OA under dry conditions ($T_{g,org}$) is calculated by the Gor-
 51 don-Taylor equation (Gordon and Taylor, 1952) by assuming the Gordon-Taylor constant (k_{GT})
 52 of 1 (Dette et al., 2014)::

$$T_{g,org} = \sum_i \omega_i T_{g,i} \quad (S3)$$

54 where ω_i represents the mass fraction of each OA species in CMAQ.

55
56 The glass transition temperature of the organic-water mixture ($T_{g,\omega_{org}}$) is determined using the
57 Gordon-Taylor equation, as expressed in Equation (S4):

58

$$T_{g,\omega_{org}} = \frac{(1-\omega_{org})T_{g,w} + \frac{1}{k_{GT}}\omega_{org}T_{g,org}}{(1-\omega_{org}) + \frac{1}{k_{GT}}\omega_{org}} \quad (S4)$$

59 where $k_{GT} = 2.5$ is assumed, and $T_{g,w}$ (the glass transition temperature of water) is set to 136
 60 K (Kohl et al., 2005). The mass fraction of OA in the particulate phase (ω_{org}) is given by
 61 Equation S5:

62

$$\omega_{org} = \frac{m_{OA}}{m_{OA} + m_{H_2O}} \quad (S5)$$

63 The mass concentration of water (m_{H_2O}) can be determined from the effective hygroscopicity
 64 parameter (κ) of OA:

65

$$m_{H_2O} = \left(\frac{a_w}{1-a_w} \right) \frac{\kappa \rho_w m_{OA}}{\rho_{OA}} \quad (S6)$$

66

$$\kappa_{org,i} = 0.11 \frac{OM}{OC} - 0.10 \quad (S7)$$

67 Here, the κ_{org} of each species was parameterized as a function of OM/OC is used (Pye et al.,
 68 2017). ρ_w (water density) and ρ_{OA} (OA density) are assumed to be 1 and 1.44 g cm^{-3} , re-
 69 spectively, based on observational experiments in DY. The water activity (a_w) is derived from
 70 the relative humidity (RH) as $a_w = RH/100$.

71
 72

73 **Supplementary Tables**74 **Table S1** Statistical metrics of meteorological parameters in DY and GZ.

Parameter	Metrics	DY	GZ	Benchmark
T2 (°C)	OBS	12.99	24.34	
	SIM	13.00	24.32	
	MB	0.01	0.01	$\leq\pm 0.5$
	ME	2.00	1.79	≤ 2
	RMSE	2.55	2.39	
RH (%)	OBS	49.14	68.07	
	SIM	46.91	64.20	
	MB	-2.23	-3.87	
	ME	9.79	8.66	
	RMSE	12.87	11.22	
WS (m/s)	OBS	3.82	2.45	
	SIM	5.17	3.19	
	MB	1.34	0.74	$\leq\pm 0.5$
	ME	1.98	1.27	≤ 2
	RMSE	2.45	1.59	≤ 2
WD (°)	OBS	159.33	94.64	
	SIM	151.39	66.41	
	MB	155.51	63.97	$\leq\pm 10$
	ME	155.52	64.03	$\leq\pm 30$
	RMSE	181.78	107.52	

75 ^a $MB = \frac{1}{N} \sum_{i=1}^N (M_i - O_i)$; $ME = \frac{1}{N} \sum_{i=1}^N |M_i - O_i|$; $RMSE = \left[\frac{1}{N} \sum_{i=1}^N (M_i - O_i)^2 \right]^{\frac{1}{2}}$, where M_i
 76 and O_i represent model predictions and observations, respectively, and N is the number of data.

77 The benchmarks refer to Emery and Tai (2001).

78

79

Table S2 Statistical metrics of predicted O₃, NO₂ and PM_{2.5} in DY and GZ.

Site	Pollutant	Case	NMB	NME	r
DY	MDA8 O ₃	1D-VBS	-0.09	0.18	0.82
		1D-VBS_E	-0.09	0.18	0.82
		1D-VBS_EY	-0.08	0.18	0.82
		2D-VBS	-0.09	0.18	0.82
DY	NO ₂	1D-VBS	-0.26	0.49	0.53
		1D-VBS_E	-0.27	0.50	0.53
		1D-VBS_EY	-0.27	0.49	0.53
		2D-VBS	-0.27	0.49	0.53
DY	PM _{2.5}	1D-VBS	-0.58	0.58	0.82
		1D-VBS_E	-0.50	0.50	0.84
		1D-VBS_EY	-0.46	0.46	0.84
		2D-VBS	-0.46	0.46	0.83
GZ	MDA8 O ₃	1D-VBS	0.26	0.49	0.38
		1D-VBS_E	0.25	0.49	0.38
		1D-VBS_EY	0.25	0.48	0.38
		2D-VBS	0.26	0.49	0.38
GZ	NO ₂	1D-VBS	-0.42	0.53	0.33
		1D-VBS_E	-0.42	0.53	0.33
		1D-VBS_EY	-0.42	0.53	0.33
		2D-VBS	-0.42	0.53	0.33
GZ	PM _{2.5}	1D-VBS	-0.48	0.50	0.33
		1D-VBS_E	-0.35	0.40	0.37
		1D-VBS_EY	-0.19	0.32	0.37
		2D-VBS	-0.31	0.38	0.45

81 ^aBenchmark values are NMB<±0.15, NME<0.25, and R>0.5 for MDA8 O₃, NMB<±0.3,

82 NME<0.5, and R>0.4 for 24-hr average PM_{2.5}, $NMB = \frac{\sum_{i=1}^N (M_i - O_i)}{\sum_{i=1}^N O_i}$; $NME = \frac{\sum_{i=1}^N |M_i - O_i|}{\sum_{i=1}^N O_i}$; $r =$

83 $\frac{\sum_{i=1}^N [(M_i - \bar{M}) \times (O_i - \bar{O})]}{\sqrt{\sum_{i=1}^N (M_i - \bar{M})^2 \times \sum_{i=1}^N (O_i - \bar{O})^2}}$, where M_i and O_i represent model predictions and observations, \bar{M}
84 and \bar{O} represent the mean of predictions and observations, and N is the number of data (Emery
85 et al., 2017).
86

87 **Table S3** Source-specific scaling factors for emissions of L/SVOCs ($\log_{10}C^*(\mu\text{g m}^{-3}) \leq 2$) derived from POA emissions, and IVOCs ($3 \leq \log_{10}C^*(\mu\text{g m}^{-3}) \leq 6$)
88 derived from VOC emissions in this study.

Sector	Subsector	Fractions for $\log C^*(\mu\text{g m}^{-3}, \text{at } 298\text{K})$ bins									Ref.	
		$f_{L/SVOC,i,j}$					$f_{IVOC,i,j}$					
		-2	-1	0	1	2	3	4	5	6		
Power	Power plants	0.2443	0.1304	0.0727	0.1454	0.4071	0.1880	0.1500	0.2260	0.1130		
	industrial boiler	0.2443	0.1304	0.0727	0.1454	0.4071	0.1880	0.1500	0.2260	0.1130		
	heat supply										Chang et al. (2022)	
	Cement											
	Coking	0.2355	0.1742	0.0805	0.0806	0.4291	0.0082	0.0075	0.0025	0.0017		
	Iron and steel											
Industry	Petrochemicals											
	Oil and gas storage	0.0000	0.0000	0.0000	0.0000	0.0000	0.0000	0.0000	0.0000	0.12	^a	
	Industrial Painting					0.0025 ^c	0.0127	0.0329	0.0405	0.1645	Mcdonald	
	architectural coating	0.0000	0.0000	0.0000	0.0000	0.0022 ^c	0.0119	0.0290	0.0358	0.1455	et al.	
	printing					0.0021 ^c	0.0103	0.0269	0.0331	0.1346	(2018)	
	Other industrial sectors	0.5430	0.0958	0.0468	0.0614	0.2531	0.0385	0.0410	0.0563	0.1132	^b	

	Domestic combustion	0.1072	0.2914	0.0377	0.0708	0.4928	0.0390	0.3170	0.2540	0.1200	
resident	Domestic biomass combustion	0.4395	0.1923	0.0680	0.1387	0.1615	0.0690	0.1710	0.0480	0.0700	Chang et al. (2022)
	Domestic VCP	0.0000	0.0000	0.0000	0.0000	0.0030 ^c	0.0156	0.0383	0.0469	0.1926	
	Other domestic sources	0.5156	0.1612	0.0352	0.0698	0.2181	0.0412	0.1754	0.1163	0.1275	^b
	Gasoline Vehicles	0.9869	0.0000	0.0031	0.0051	0.0045	0.0061	0.0206	0.0568	0.0943	Tang et al. (2021)
Transportation	Diesel Vehicles	0.1321	0.0546	0.0858	0.3641	0.3633	0.0540	0.1490	0.1870	0.1590	^d
	Motorcycles	0.9869	0.0000	0.0031	0.0051	0.0045	0.0061	0.0206	0.0568	0.0943	Tang et al. (2021)
	Non-Road transportation	0.7801	0.0307	0.0399	0.0645	0.0849	0.0147	0.0344	0.0684	0.0787	^f
Agriculture	Fertilizer Application	0.0000	0.0000	0.0000	0.0000	0.0000	0.0000	0.0000	0.0000	0.0000	Chang et al. (2022)
	Livestock Farming										

89 ^a Data from the California Air Resources Board's 2015 Consumer and Commercial Products Survey (CARB, 2019);

90 ^b Average values of subsectors under the same sector;

91 ^c Since volatile chemical product emissions are closely correlated with VOC emissions, the SVOC emissions for this sector were estimated based on VOC
92 emissions.

93 ^d The IVOC scaling factors for diesel vehicles were referenced from Lu et al. (2020) , while the SVOC scaling factors were based on the work of An et al.
94 (2023).

95 ^f For non-road mobile sources, scaling factors for agricultural machinery (Che et al., 2023) , road construction machinery (Shen et al., 2023), and ships (An et
96 al., 2023), were used. The contributions of different sources to non-road mobile sources were obtained from Huang et al. (2018) and Zhao et al. (2022).

97 **Table S4** Annual emissions of IVOCs and SVOCs (Unit: Tg) from different emission sources
98 in China in 2018.

Sector	IVOCs	SVOCs
Industry and Power	1.17	0.34
Residential	1.91	2.69
Transportation	0.90	0.15
Solvent use	2.69	/
Total	6.68	3.18

99

100 **Table S5** Mole-based SOA yields for aromatics and PAHs used in this study.

Case	Precur-sor	High NOx						Ref	
		10E-06	0.01	0.1	1	10	100		
1D-VBS	Benzene	0.0000	0.0000	0.0000	0.0340	0.0000	0.3920	Qin et al. (2021)	
	Toluene	0.0000	0.0000	0.0000	0.0160	0.0510	0.0470		
	Xylene	0.0000	0.0000	0.0000	0.0150	0.0230	0.0600		
	PAHs	0.0000	0.0000	0.0000	0.0280	0.0225	0.0280		
1D-VBS_E_Y	Precur-sor	Low NOx						Ref	
		10E-06	0.01	0.1	1	10	100		
	Benzene	0.0000	0.1460	0.0000	0.0000	0.0000	0.0000	Qin et al. (2021)	
	Toluene	0.0000	0.1400	0.0000	0.0000	0.0000	0.0000		
1D-VBS_E_Y	Xylene	0.0000	0.1930	0.0000	0.0000	0.0000	0.0000	Bilsback et al. (2023)	
	PAHs ^a	0.0000	0.0473	0.0000	0.0000	0.0000	0.0000		
	Precur-sor	High NOx							
		10E-06	0.01	0.1	1	10	100		
1D-VBS_E_Y	Benzene	0.0000	0.0000	0.1874	0.1559	0.0000	0.0000	Bilsback et al. (2023)	
	Toluene	0.0000	0.0000	0.1358	0.0967	0.0000	0.0000		
	Xylene	0.0000	0.0000	0.0284	0.0049	0.0040	0.1581		
	PAHs ^a	0.0000	0.1183	0.0988	0.1269	0.2110	0.0000		
1D-VBS_E_Y	Precur-sor	Low NOx						Ref	
		10E-06	0.01	0.1	1	10	100		
	Benzene	0.0017	0.0131	0.0000	0.0592	0.1732	0.0000	Bilsback et al. (2023)	
	Toluene	0.0007	0.0299	0.0000	0.0703	0.1584	0.0000		
1D-VBS_E_Y	Xylene	0.0106	0.0000	0.1452	0.0000	0.0422	1.3439	Bilsback et al. (2023)	
	PAHs ^a	0.0230	0.0600	0.0381	0.0572	0.1753	0.0000		

101 ^a The parameters for PAHs adopted naphthalene SOA yields from Bilsback et al. (2023).

102

103 **Table S6** Summary of O/C ratios for POA factors in eastern China reported in prior measure-
 104 ments.

Site	HOA	BBOA	CCOA	COA	NOA	Ref
Dongying	0.55	0.37	/	/	/	Feng et al. (2023)
Guangzhou	0.2	/	/	0.19	0.5	Chen et al. (2021)
Gucheng	0.13	0.44	0.15	/	/	Zhang et al. (2022)
Beijing	0.16	0.29	0.19	0.16	/	Xu et al. (2021)
Nanjing	0.12	/	/	0.27	/	Xian et al. (2023)
Nanjing	0.17	0.49	/	/	/	Gu et al. (2022)
Shanghai	0.15	/	/	0.29	/	Zhu et al. (2021)
Hangzhou	0.07	/	/	0.18/	/	Li et al. (2018)
Yangzhou	0.25	0.45	/	0.36	/	(Ge et al., 2017)
Average	0.2	0.41	0.17	0.24	0.5	

105

106 **Table S7** OA surrogate species in the 1D-VBS and their physicochemical properties at 298K,
 107 including saturated vapor pressure (C_0^*), organic matter to organic carbon ratio (OM/OC), mo-
 108 lecular weight (\tilde{M}), and oxygen to carbon ratio (O/C).

Species	Description	C_0^*	OM/OC	\tilde{M}	O/C	Ref
AAVB1	ASOA	0.01	2.7	198.0	1.227	Qin et al. (2021)
AAVB2		1	2.35	179.0	0.947	
AAVB3		10	2.17	169.0	0.803	
AAVB4		100	1.99	158.0	0.659	
AAVB5 ^a		0.1	2.53	189.0	1.091	
AAVB6 ^a		1E-06	3.41	229.0	1.797	Newly added
AOLGA	Oligomers derived from ASOA	1E-10	2.50	206.0	1.067	Pye et al. (2017)
AIETET	2-methyltetrols (2-MT)	1E-10	2.27	136.15	0.833	
AIEOS	IEPOX-derived organic sulfates	1E-10	3.60	216.2	1.947	
AIMGA	2-methylglyceric acid (2-MG)	1E-10	2.50	120.1	1.067	Pye et al. (2013)
AIMOS	MPAN-derived organic nitrates	1E-10	4.17	200.16	2.403	
ADIM	Dimers	1E-10	2.07	248.23	0.723	
AISO1	Semi-volatile isoprene SOA	116.01	2.20	132.0	0.827	
AISO2	Semi-volatile SOA from isoprene dinitrates produced from NO ₃ reaction	0.617	2.23	133.0	0.857	
AISOPNN		8.9	3.80	226.0	2.107	Pye et al. (2015)
AMT1		0.01	1.67	300.0	0.4	
AMT2		0.1	1.67	200.0	0.4	
AMT3	Monoterpene SOA from OH/O ₃ -initiated oxidation	1	1.72	186.0	0.444	Xu et al. (2018)
AMT4	10	1.53	184.0	0.3		
AMT5	100	1.57	170.0	0.333		
AMT6	1000	1.40	168.0	0.2		
AMTNO3	Semi-volatile SOA from	12.0	1.90	231.0	0.587	Pye et al. (2015)

		monoterpene nitrates (excluding α -pinene)					
		Nonvolatile organic hydrolysis					
AMTHYD	product of MTNO ₃ ^b and ISOPNN ^c	1E-10	1.54	186.0	0.299		
ASQT	Sesquiterpene SOA	24.984	1.52	273.0	0.283	Carlton et al. (2010); Pye et al. (2017)	
AOLGB	oligomers derived from BSOA	1E-10	2.10	248.0	0.747	Carlton et al. (2010); Pye et al. (2017)	
AGLY	OA from glyoxal and methylglyoxal uptake onto accumulation-mode particles	1E-10	2.13	66.4	0.771	Pye et al. (2015)	
AORG C	OA from aqueous-phase oxidation of glyoxal and methylglyoxal in cloud droplets	1E-10	2.00	177.0	0.677	Carlton et al. (2008)	
APNCOM	Non-carbon fraction of POA	1E-10	1.60	220.0	0.347	Simon and Bhave (2012)	
APOC	Carbon fraction of POA						
ALVPO1		0.1	1.39	218.0	0.185		
ASVPO1		1	1.32	230.0	0.123		
ASVPO2		10	1.26	241.0	0.073		
ASVPO3		100	1.21	253.0	0.032		
AIVPO1	Semi-volatile	1000	1.17	266.0	0.00	Murphy et al. (2017)	
ALVOO1	POA	0.01	2.27	136.0	0.886		
ALVOO2		0.1	2.06	136.0	0.711		
ASVOO1		1	1.88	135.0	0.567		
ASVOO2		10	1.73	135.0	0.477		
ASVOO3		100	1.60	134.0	0.345		

110 ^b MTNO₃: Monoterpene-derived organic nitrates.

111 ^c ISOPNN: Second generation isoprene dinitrate from NO₃ reaction

112 .

113 **Table S8** OA surrogate species in the 2D-VBS and their physicochemical properties at 298 K
 114 (Zhao et al., 2015; Chang et al., 2022), including saturated vapor pressure (C_o^*), organic matter
 115 to organic carbon ratio (OM/OC), molecular weight (\tilde{M}), and oxygen to carbon ratio (O/C).

Species	C_o^*	OM/OC	\tilde{M}	O/C
AM120	0.01	3.667	152.30	2.0
A0020	1	3.667	141.00	2.0
A0120	10	3.667	129.70	2.0
A0220	100	3.667	118.50	2.0
A0320	1000	3.667	107.20	2.0
A0420	1.0E+04	3.667	95.90	2.0
A0520	1.0E+05	3.667	84.60	2.0
A0620	1.0E+06	3.667	73.30	2.0
A0720	1.0E+07	3.667	62.10	2.0
AM115	0.01	3.041	161.60	1.5
A0015	1	3.041	149.60	1.5
A0115	10	3.041	137.60	1.5
A0215	100	3.041	125.70	1.5
A0315	1000	3.041	113.70	1.5
A0415	1.0E+04	3.041	101.70	1.5
A0515	1.0E+05	3.041	89.80	1.5
A0615	1.0E+06	3.041	77.80	1.5
A0715	1.0E+07	3.041	65.80	1.5
AM110	0.01	2.417	178.00	1.0
A0010	1	2.417	164.80	1.0
A0110	10	2.417	151.60	1.0
A0210	100	2.417	138.40	1.0
A0310	1000	2.417	125.20	1.0
A0410	1.0E+04	2.417	112.00	1.0
A0510	1.0E+05	2.417	98.90	1.0
A0610	1.0E+06	2.417	85.70	1.0
A0710	1.0E+07	2.417	72.50	1.0
AM107	0.01	2.042	195.70	0.7
A0007	1	2.042	181.20	0.7
A0107	10	2.042	166.70	0.7
A0207	100	2.042	152.20	0.7
A0307	1000	2.042	137.70	0.7

A0407	1.0E+04	2.042	123.20	0.7
A0507	1.0E+05	2.042	108.70	0.7
A0607	1.0E+06	2.042	94.20	0.7
A0707	1.0E+07	2.042	79.70	0.7
AM104	0.01	1.667	228.80	0.4
A0004	1	1.667	211.90	0.4
A0104	10	1.667	194.90	0.4
A0204	100	1.667	178.00	0.4
A0304	1000	1.667	161.00	0.4
A0404	1.0E+04	1.667	144.10	0.4
A0504	1.0E+05	1.667	127.10	0.4
A0604	1.0E+06	1.667	110.20	0.4
A0704	1.0E+07	1.667	93.20	0.4
AM102	0.01	1.417	273.20	0.2
A0002	1	1.417	253.00	0.2
A0102	10	1.417	232.70	0.2
A0202	100	1.417	212.50	0.2
A0302	1000	1.417	192.30	0.2
A0402	1.0E+04	1.417	172.00	0.2
A0502	1.0E+05	1.417	151.80	0.2
A0602	1.0E+06	1.417	131.50	0.2
A0702	1.0E+07	1.417	111.30	0.2
AM101	0.01	1.292	312.30	0.1
A0001	1	1.292	289.20	0.1
A0101	10	1.292	266.00	0.1
A0201	100	1.292	242.90	0.1
A0301	1000	1.292	219.80	0.1
A0401	1.0E+04	1.292	196.60	0.1
A0501	1.0E+05	1.292	173.50	0.1
A0601	1.0E+06	1.292	150.40	0.1
A0701	1.0E+07	1.292	127.20	0.1
AM100	0.01	1.167	378.00	0.0
A0000	1	1.167	350.00	0.0
A0100	10	1.167	322.00	0.0
A0200	100	1.167	294.00	0.0
A0300	1000	1.167	266.00	0.0
A0400	1.0E+04	1.167	238.00	0.0

A0500	1.0E+05	1.167	210.00	0.0
A0600	1.0E+06	1.167	182.00	0.0
A0700	1.0E+07	1.167	154.00	0.0
ADIM	1E-10	2.07	248.23	0.723
AGLY	1E-10	2.13	66.4	0.771
AIEOS	1E-10	3.60	216.2	1.947
AIETET	1E-10	2.27	136.15	0.833
AIMGA	1E-10	2.50	120.1	1.067
AIMOS	1E-10	4.17	200.16	2.403
AISO1	116.01	2.20	132.0	0.827
AISO2	0.617	2.23	133.0	0.857
AISO3	1E-10	2.80	168.2	1.307
AISOPNN	8.9	3.80	226.0	2.107
AMTNO3	12.0	1.90	231.0	0.587
AMTHYD	1E-10	1.54	186.0	0.299
AOLGB	1E-10	2.10	248.0	0.747

116 Note: While ASOA, BSOA, and POA are separately represented in the model, species with
 117 identical volatility and O/C are assumed to share physicochemical properties and are not listed
 118 individually in this table.

119 **Table S9** Contribution of SOA to OA in different simulations.

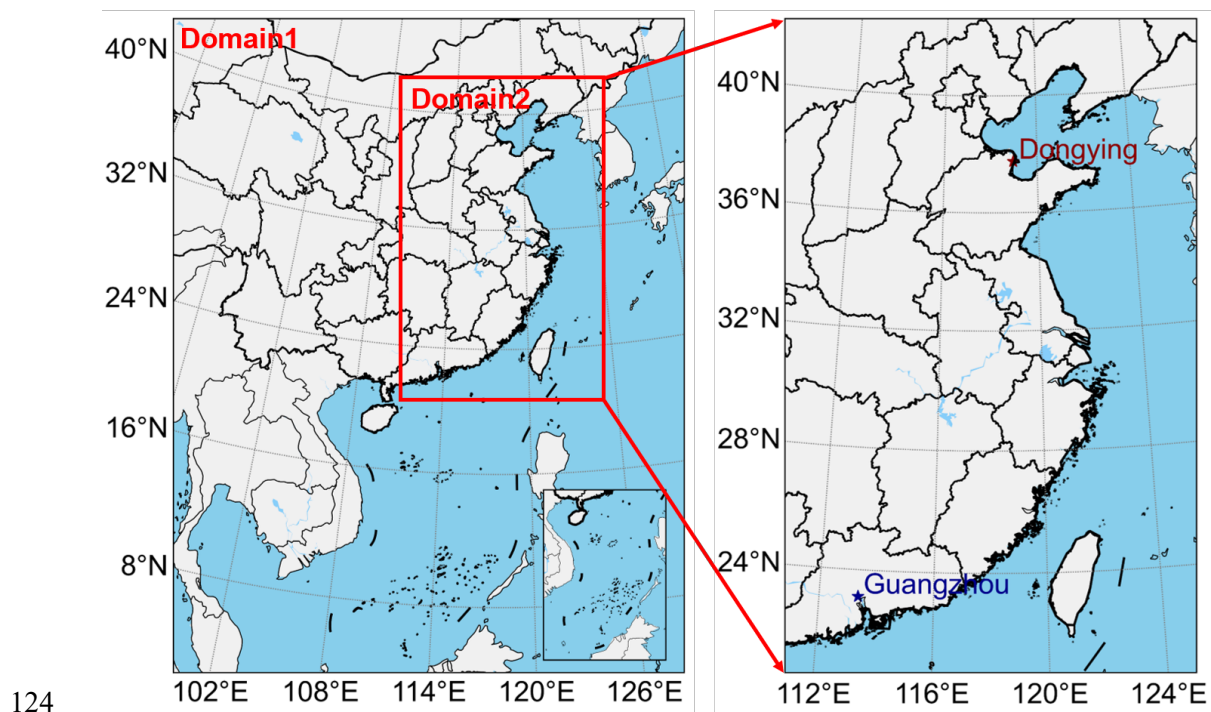
Site	Case	SIM	OBS
DY	1D-VBS	59%	
	1D-VBS_E	62%	
	1D-VBS_EY	67%	72%
GZ	2D-VBS	82%	
	1D-VBS	78%	
	1D-VBS_E	72%	
	1D-VBS_EY	77%	64%
	2D-VBS	84%	

120

121 **Table S10** CMAQ performance in OA, SOA and POA simulation.

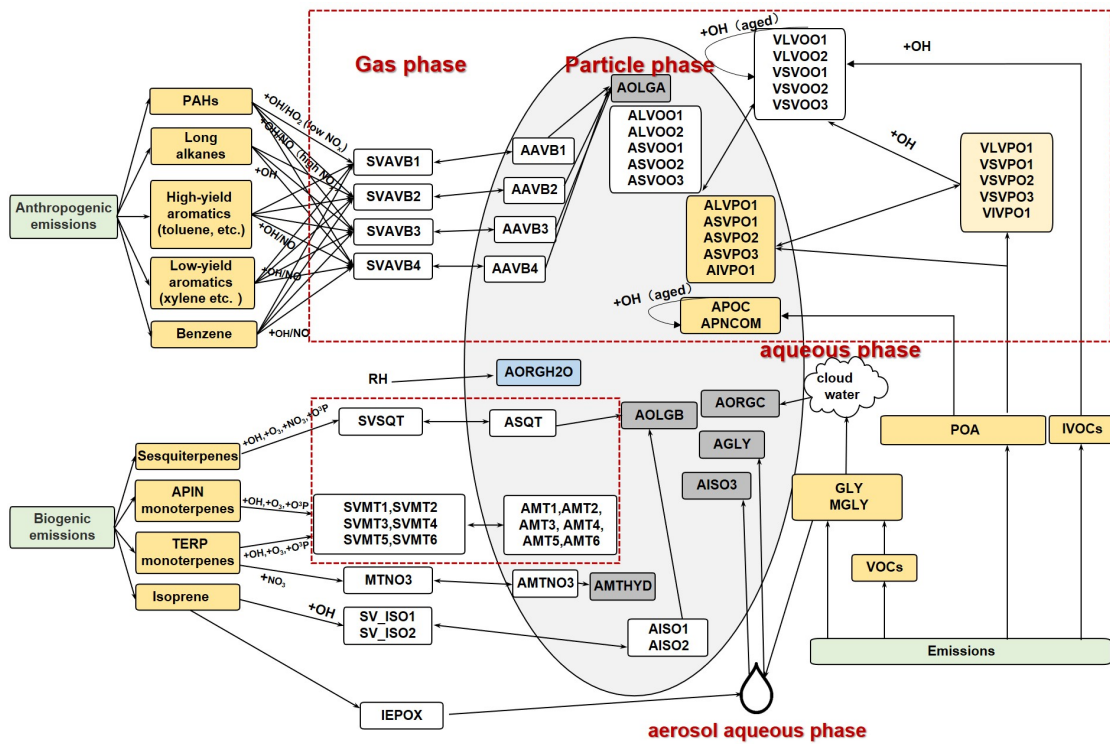
Site	Pollu- tant	Case	NMB	NME	r
DY	OA	1D-VBS	-0.67	0.67	0.87
		1D-VBS_E	-0.37	0.39	0.85
		1D-VBS_EY	-0.27	0.36	0.84
		2D-VBS	-0.24	0.38	0.83
DY	SOA	1D-VBS	-0.72	0.72	0.78
		1D-VBS_E	-0.45	0.49	0.74
		1D-VBS_EY	-0.30	0.43	0.75
		2D-VBS	-0.11	0.41	0.75
GZ	POA	1D-VBS	-0.55	0.55	0.80
		1D-VBS_E	-0.20	0.30	0.84
		1D-VBS_EY	-0.21	0.30	0.84
		2D-VBS	-0.54	0.54	0.86
GZ	OA	1D-VBS	-0.72	0.72	0.34
		1D-VBS_E	-0.44	0.48	0.33
		1D-VBS_EY	-0.34	0.41	0.33
		2D-VBS	-0.24	0.36	0.39
GZ	SOA	1D-VBS	-0.71	0.71	0.46
		1D-VBS_E	-0.47	0.48	0.44
		1D-VBS_EY	-0.33	0.39	0.43
		2D-VBS	-0.14	0.33	0.43
GZ	POA	1D-VBS	-0.76	0.76	0.05
		1D-VBS_E	-0.40	0.60	0.06
		1D-VBS_EY	-0.41	0.61	0.07
		2D-VBS	-0.53	0.60	0.35

123 **Supplementary Figures**



124
125 **Figure S1** Modeling domains and locations of observational sites Dongying (DY) and Guang-
126 zhou (GZ).

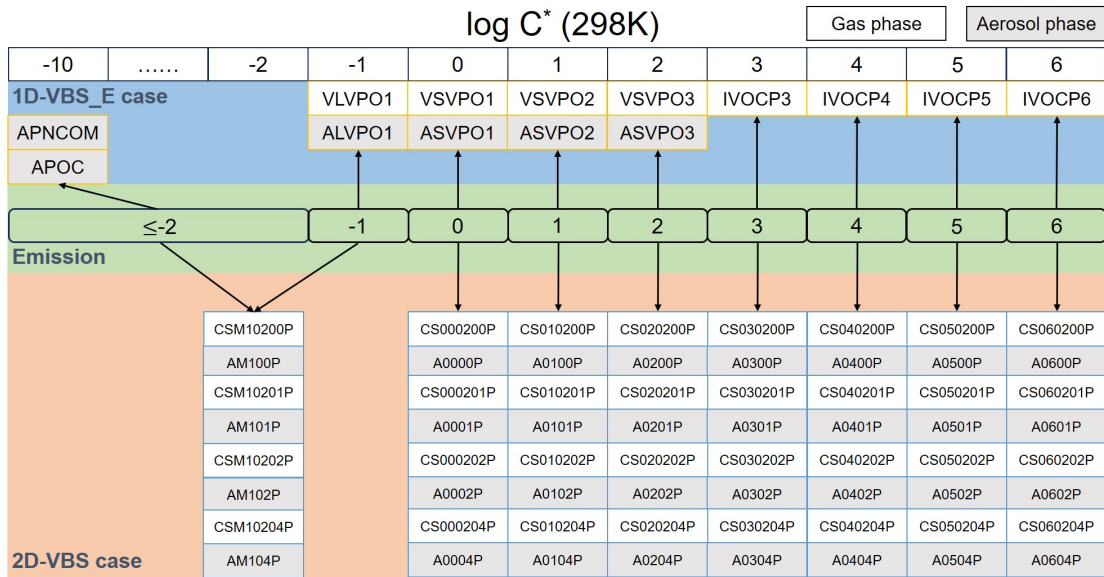
127



128

129

130 **Figure S2** Organic aerosol treatment in CMAQv5.3-aero7i. Species in grey boxes are assumed
 131 to be non-volatile. The schematic diagram is adapted from Fig.3 in Pye et al. (2017). Boxes
 132 outlined in red dashed lines indicate that SOA was represented within the 1D-VBS framework
 133 in the aero7i module, which is replaced by the 2D-VBS scheme in CMAQv5.4. SOA derived
 134 from isoprene, glyoxal, methylglyoxal, and monoterpenes+NO₃ was treated consistently in both
 135 the 1D-VBS and 2D-VBS simulations.



136

137 **Figure S3** Volatility distribution of L/S/IVOC emissions in the 1D-VBS_Y and 2D-VBS simulations. The green area shows L/S/IVOC emission estimates. The blue and orange areas represent allocation of these emissions across volatility bins in the 1D-VBS_E and 2D-VBS simulations, respectively. Grey boxes denote aerosol phase, and white boxes indicate gas phase.

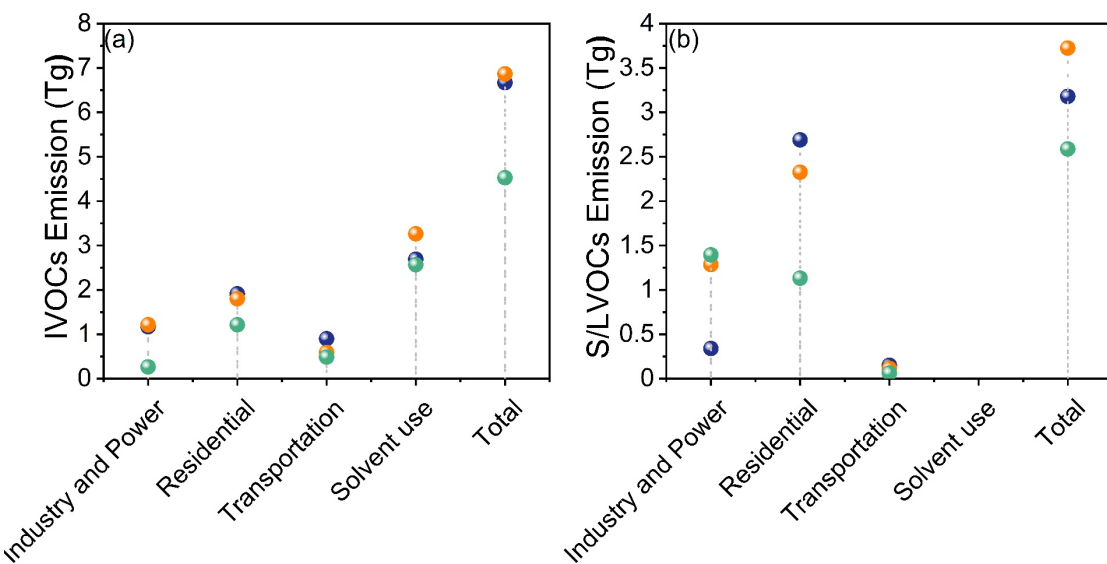
138

139

140

141

● This study ● Chen et al ● Zheng et al

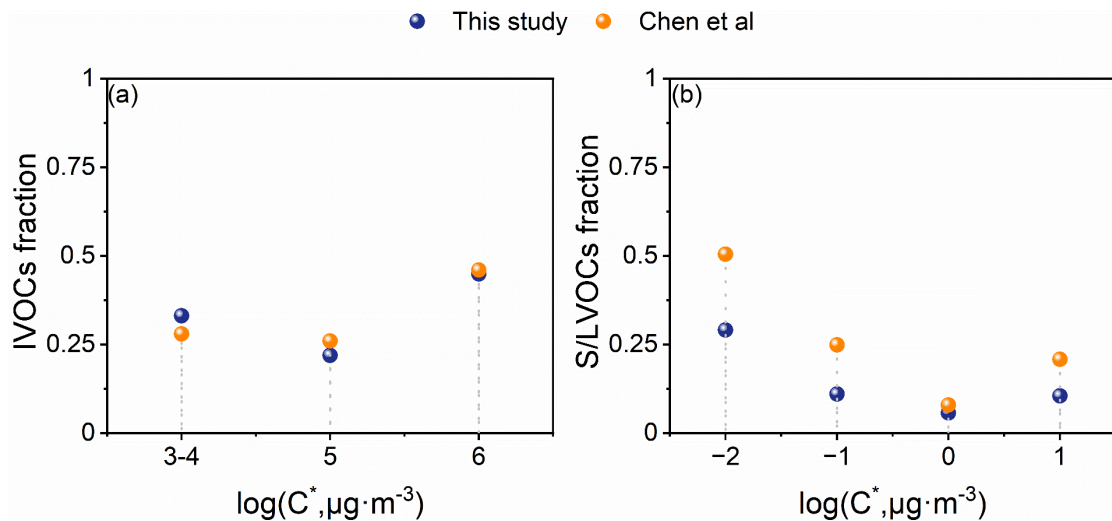


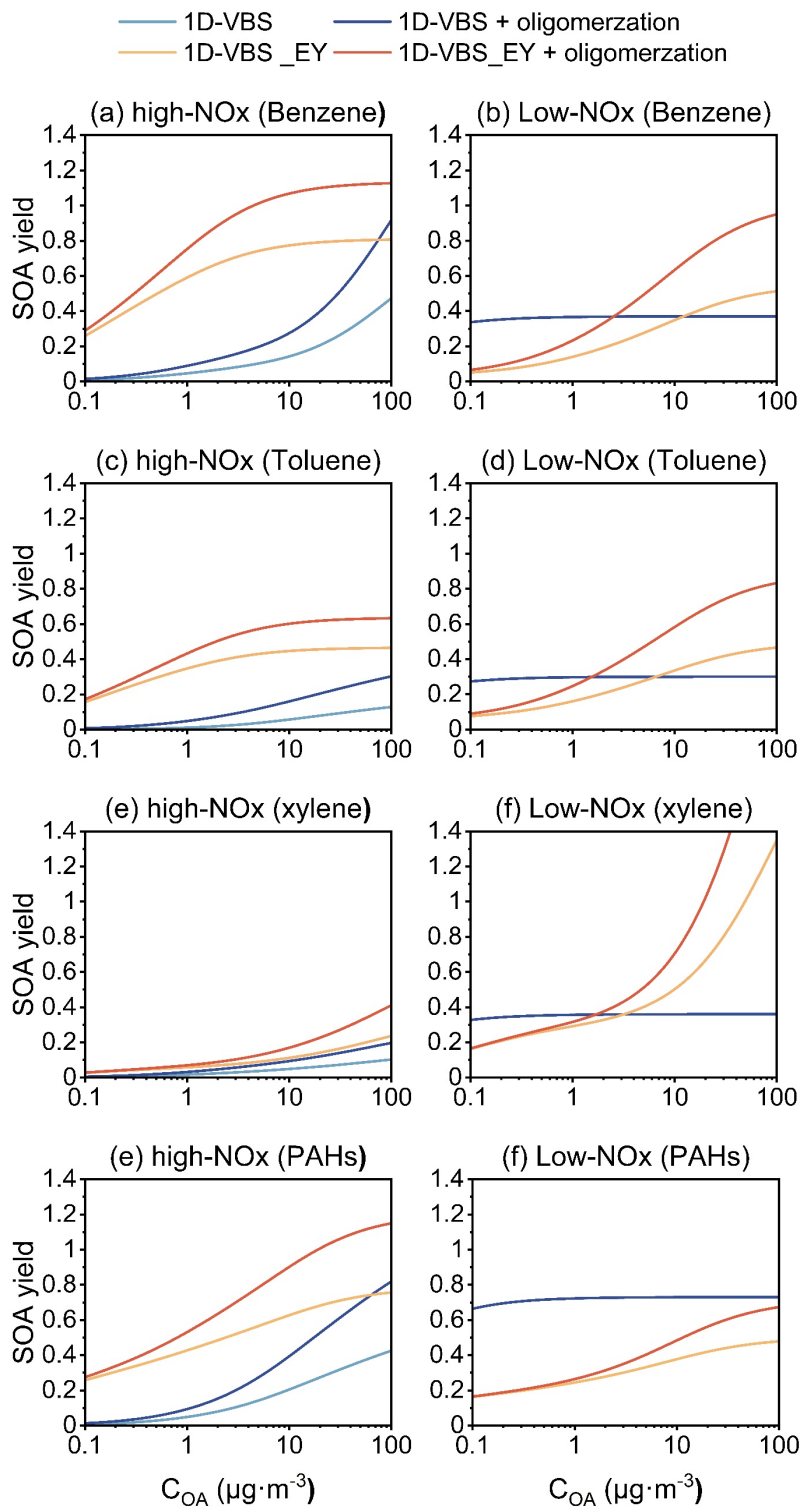
144 **Figure S4** Comparison of annual emissions of (a) IVOC and (b) S/LVOC emissions in China
145 in 2018 from this study with estimates from Chen et al. (2024a); (Chen et al., 2024b) and Feng
146 et al. (2023).

148

149 **Figure S5** Comparison of the volatility distributions of (a) IVOC and (b) S/LVOC emissions
150 across all volatility bins in China in 2018 between this study and estimates from Chen et al.
151 (2024a); (Chen et al., 2024b).

152



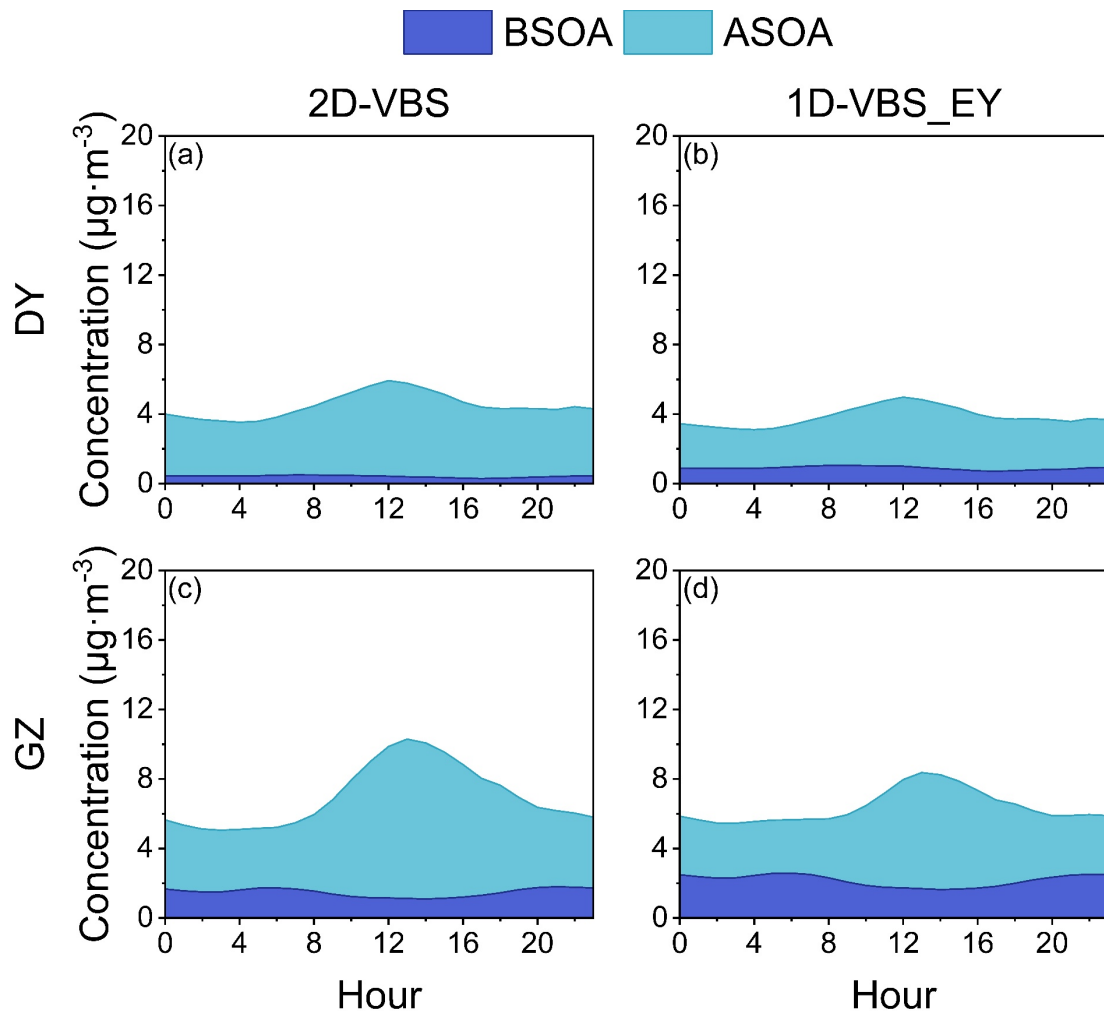


153

154 **Figure S6** SOA mass yield from aromatic hydrocarbons (a, b: benzene; c, d: toluene; e, f: xylene;

155 g,h: PAHs) under high-NOx and low-NOx conditions.

156

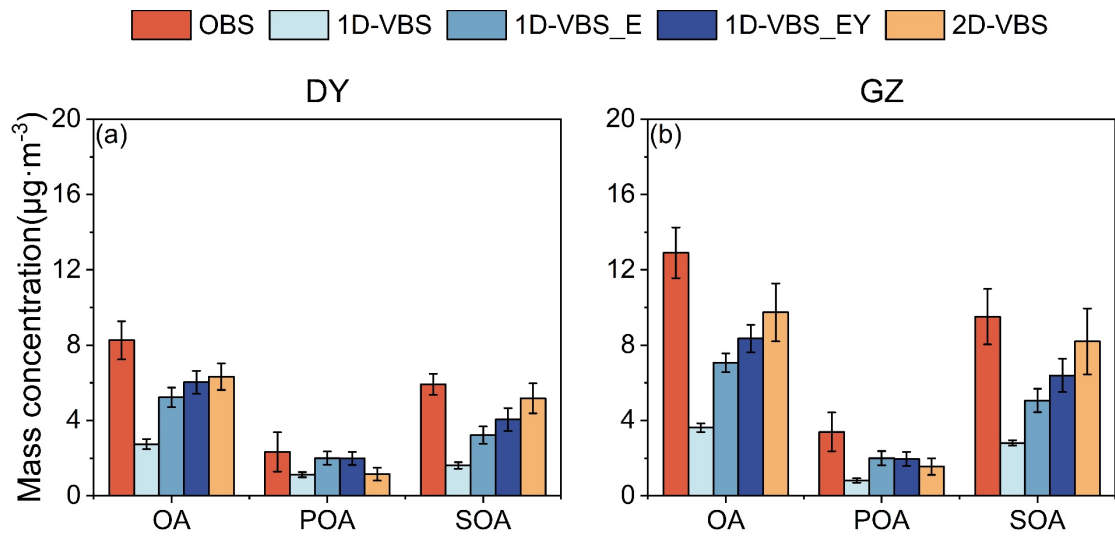


158 **Figure S7** Diurnal variations of SOA compositions (ASOA and BSOA) from 1D-VBS_E and
159 2D-VBS simulations in DY (a-b) and GZ (c-d).
160
161

162

163 **Figure S8** Period-averaged mass concentrations of modeled and observed OA, POA, and SOA
164 in DY (a) and GZ (b), with BBOA and COA excluded from the OA and POA observations.

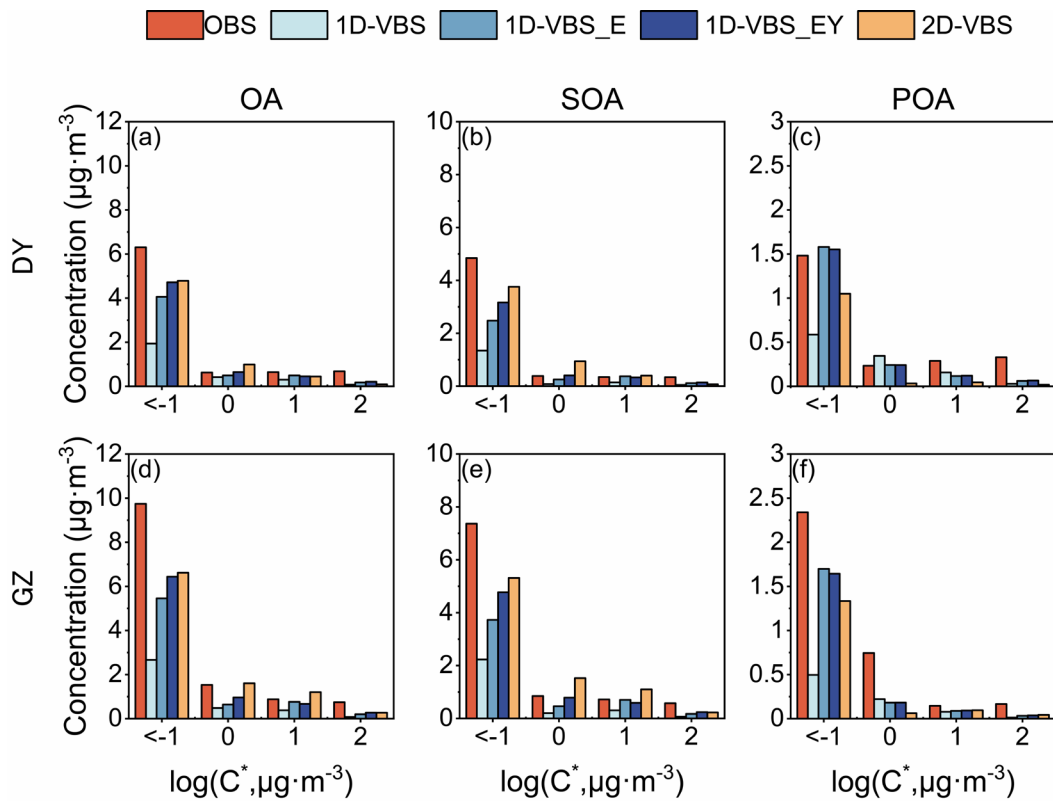
165

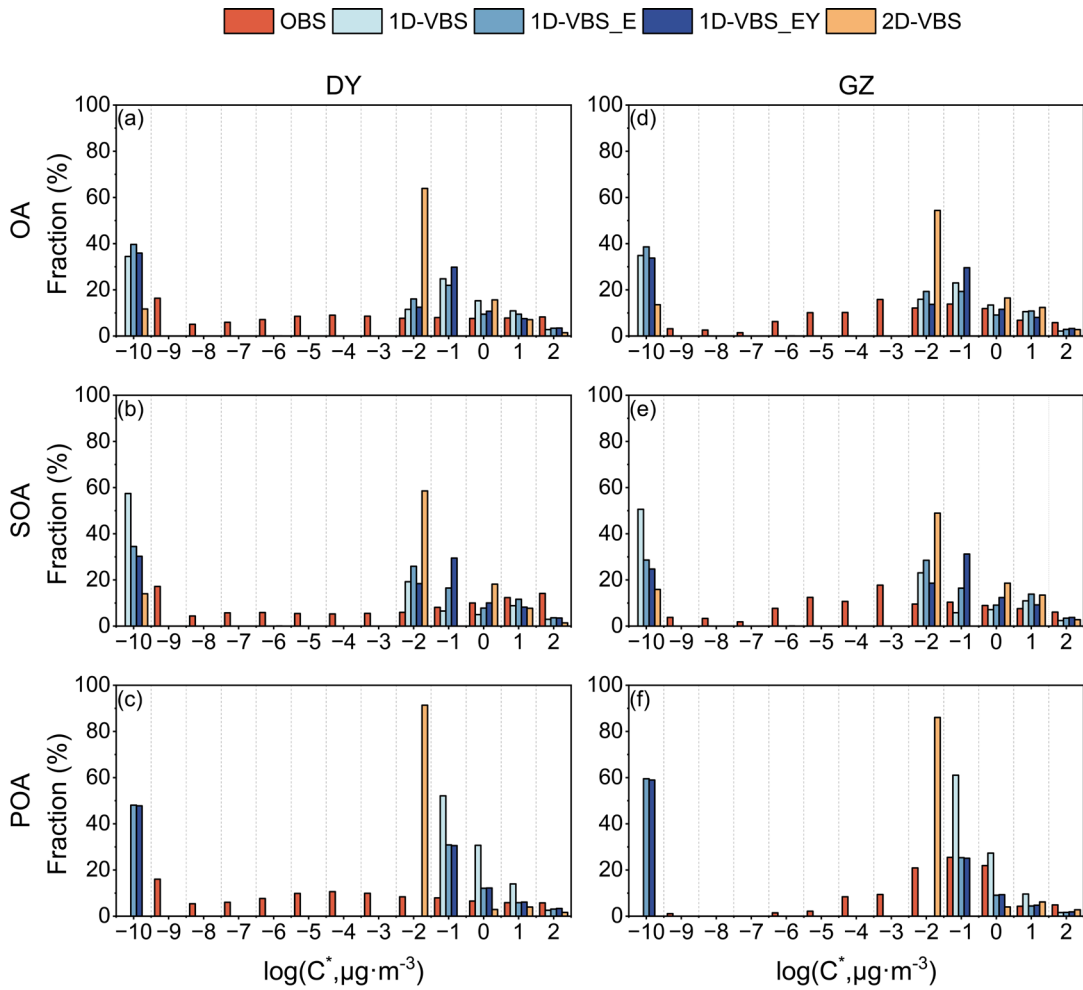


166

167 **Figure S9** Simulated mass concentrations of OA, POA, and SOA across volatility bins with C^*
 168 ranging from $<10^{-1}$ to $10^2 \mu\text{g m}^{-3}$, compared to observations in DY (a-c) and GZ (d-f).

169

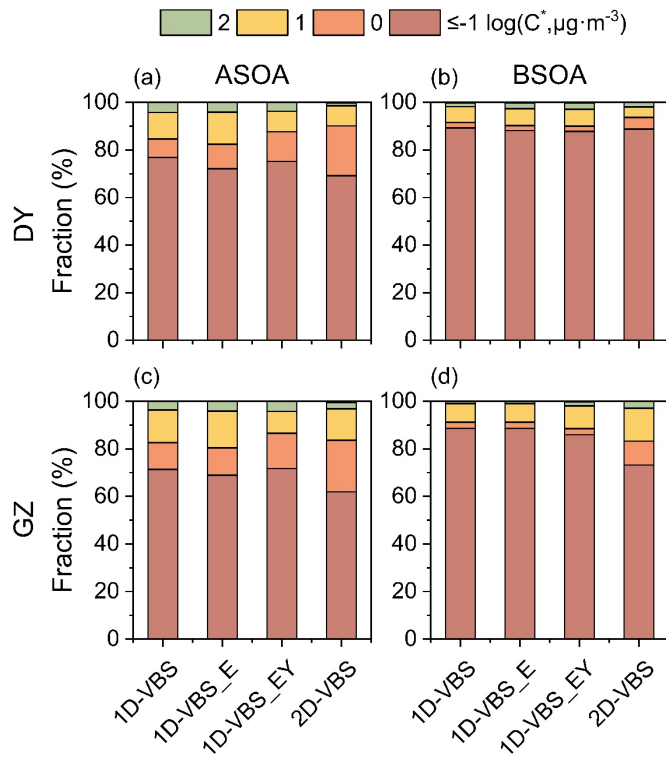




170

171 **Figure S10** Simulated OA, POA, and SOA volatility distributions across volatility bins with C^*
 172 ranging from 10^{-10} to $10^2 \mu\text{g m}^{-3}$, compared to the observations in DY (a-c) and GZ (d-f).

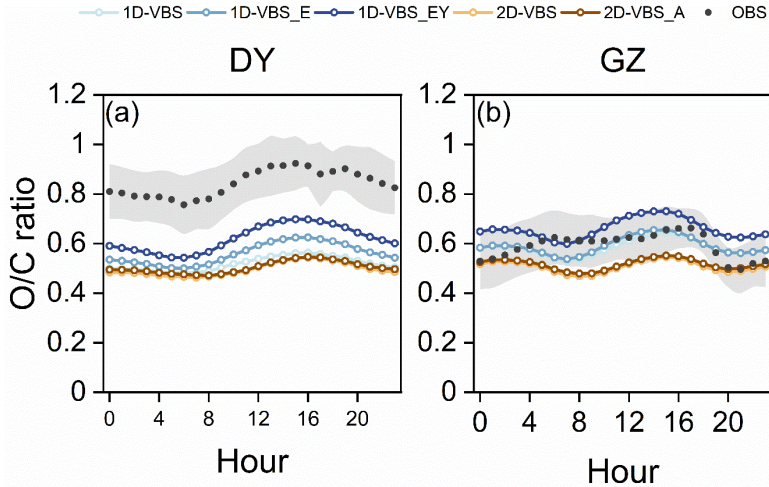
173



174

175 **Figure S11** Simulated volatility distributions of BSOA and ASOA in DY (a-b) and GZ (c-d).

176

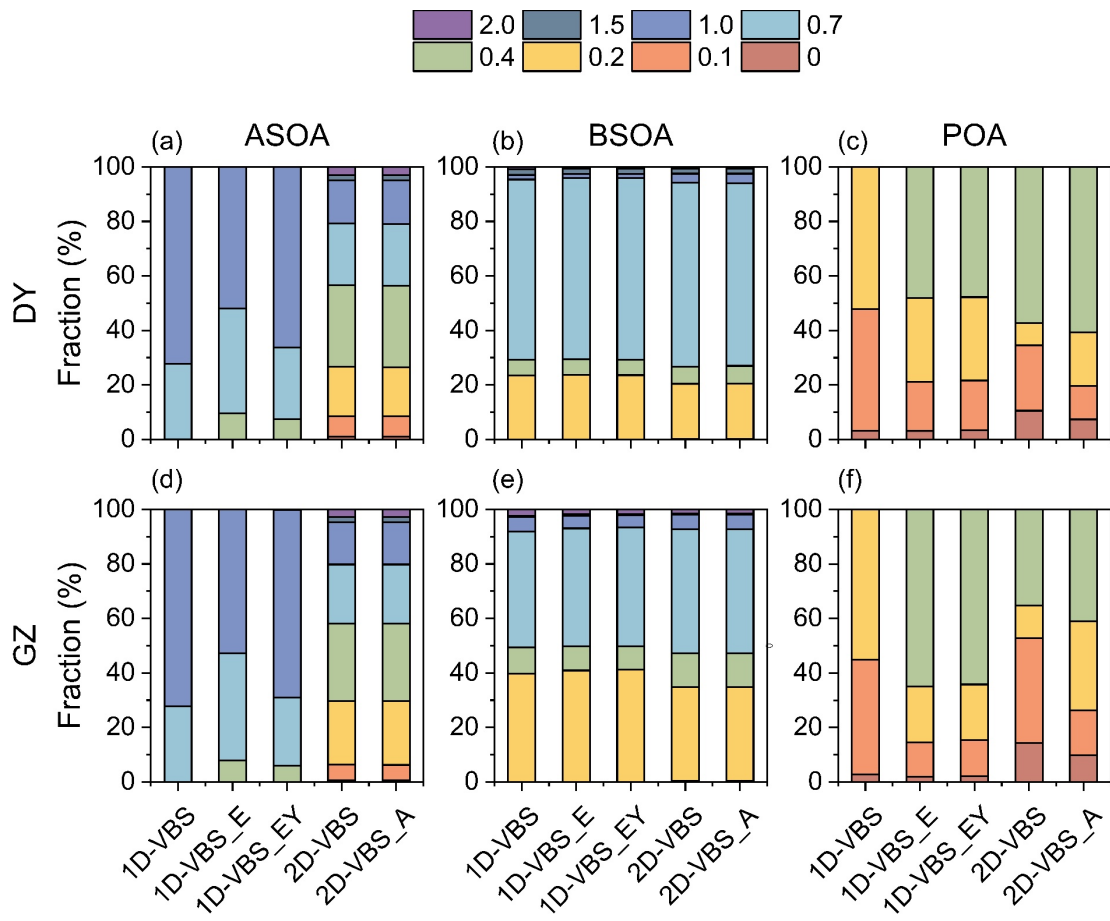


177

178 **Figure S12** Simulated diurnal variations of OA O/C ratios compared to observations in DY (a)
 179 and GZ (b).

180

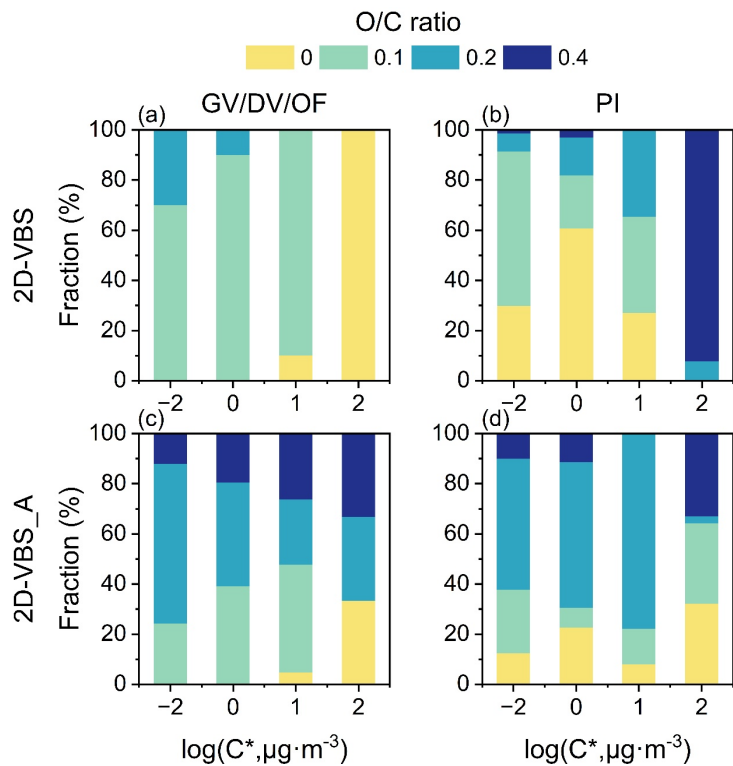
181



182

183 **Figure S13** Mass contributions of ASOA, BSOA and POA across O/C bins in DY (a-c) and
 184 GZ(d-f). The numbers in the legends represent median O/C values.

185



186

187 **Figure S14** O/C distributions of L/SVOC emissions from gasoline/diesel vehicles or off-road
 188 mobile sources (GV/DV/OF), and power plants or industrial sources (PI) in the 2D-VBS sim-
 189 ulation (a–b) and the 2D-VBS_A simulation (c–d).

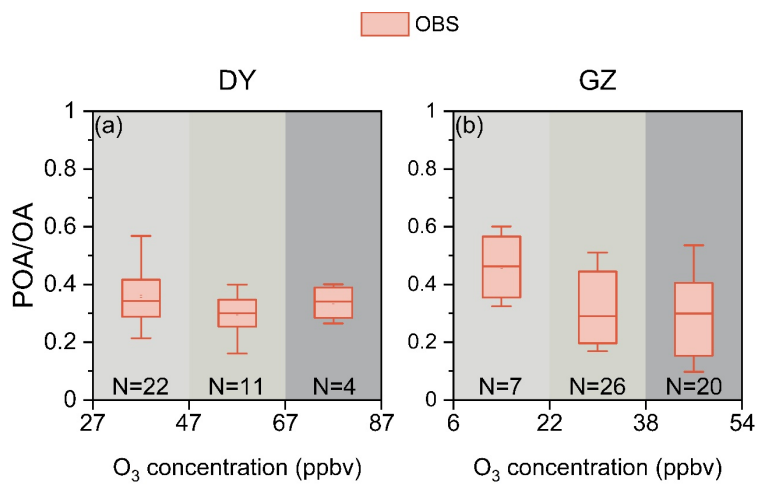


Figure S15 Variation of POA/OA ratios with daily average ozone concentrations in the observations in DY (a) and GZ (b). N denotes the sample size of POA/OA ratios within each ozone interval.

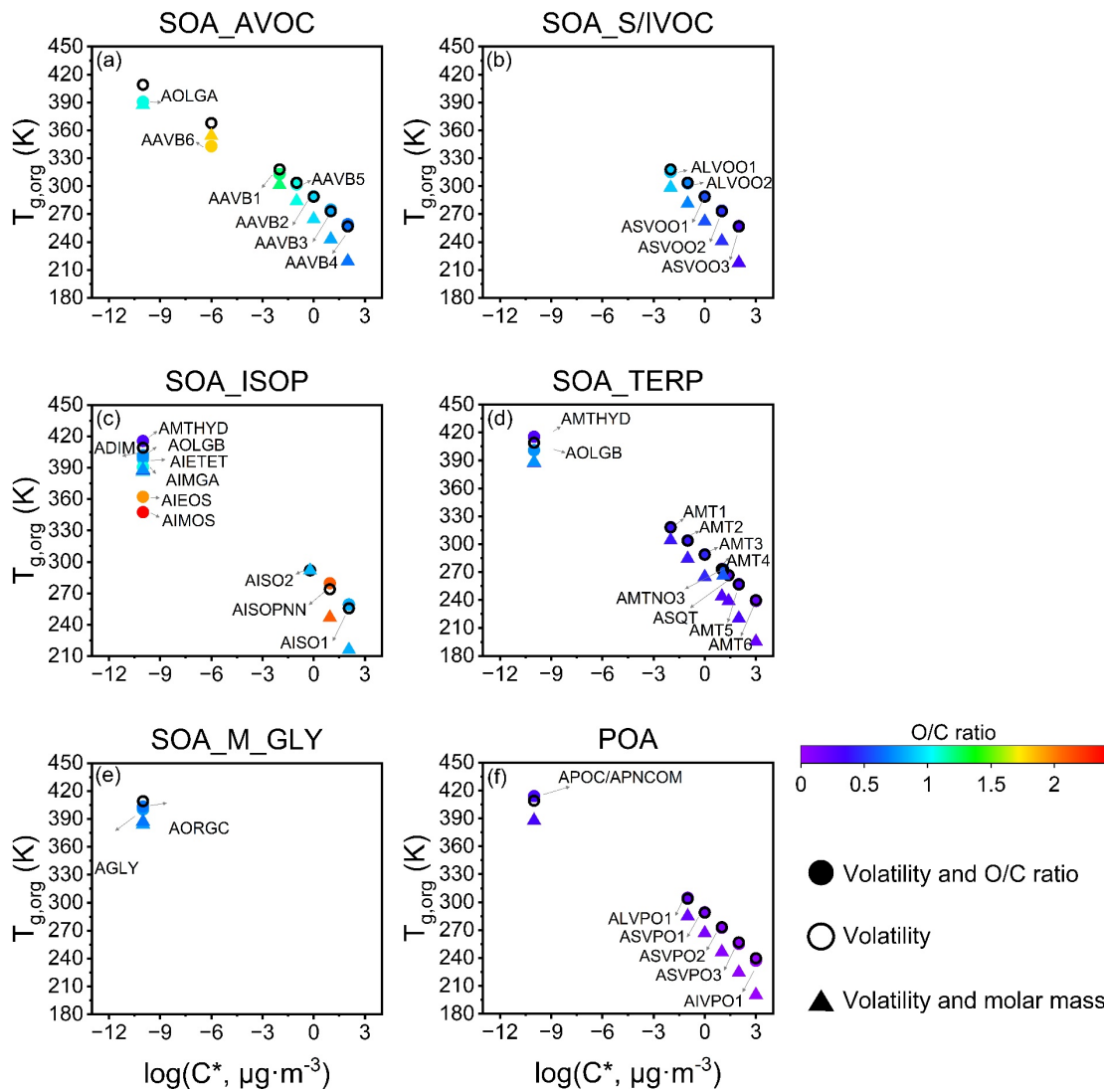


Figure S16 Estimated T_g values for OA surrogate species. Solid circles represent $T_{g,org}$ calculated using both volatility and O/C ratios, with colors indicating the O/C ratio, while open circles represent $T_{g,org}$ calculated using volatility alone and solid triangles represent $T_{g,org}$ calculated using volatility and molar mass (see Table S6 for a more detailed description of the CMAQ OA species).

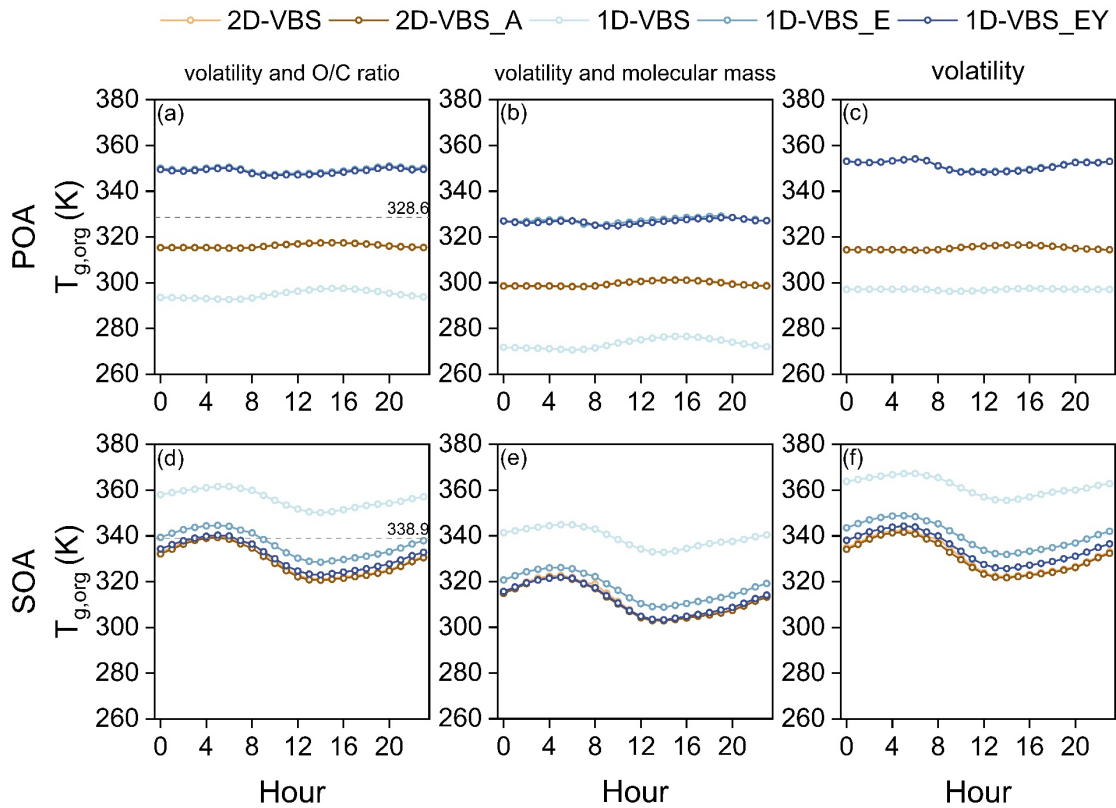


Figure S17 Comparison of simulated diurnal variations of POA and SOA $T_{g,org}$ with estimates based on observations in DY. $T_{g,org}$ values were estimated using both volatility and O/C ratios (a)(d), volatility and molecular masses (b)(e), and volatility only (c)(f), respectively.

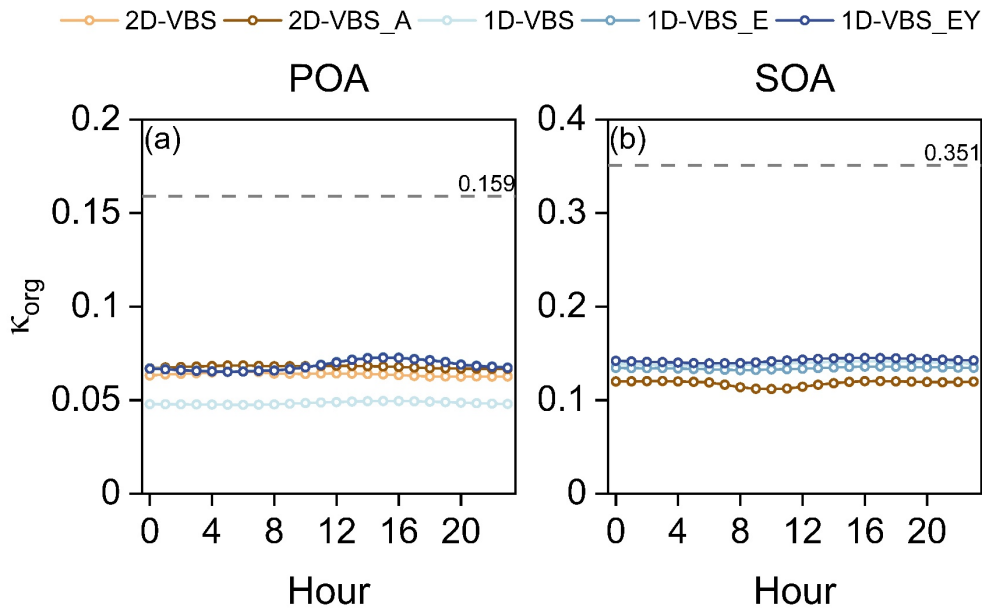


Figure S18 Diurnal variation of (a) POA and (b) SOA κ_{org} , predicted as a function of OM/OC, with the grey dashed line representing the κ_{org} value derived from observations, estimated as a function of f_{44} (i.e., the fraction of m/z 44 signal in total organic signals).

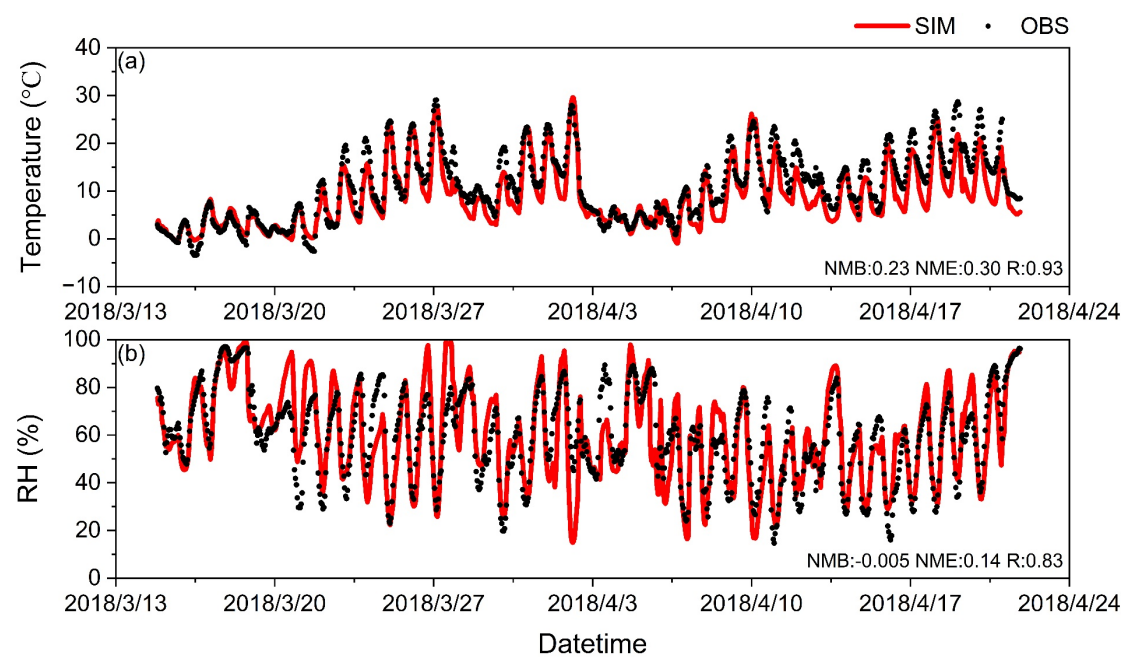


Figure S19 Time series of (a) temperature (T) and (b) relative humidity (RH) at the DY site.

Supplementary References

- An, J., Huang, C., Huang, D., Qin, M., Liu, H., Yan, R., Qiao, L., Zhou, M., Li, Y., Zhu, S., Wang, Q., and Wang, H.: Sources of organic aerosols in eastern China: a modeling study with high-resolution intermediate-volatility and semivolatile organic compound emissions, *Atmospheric Chemistry and Physics*, 23, 323-344, <https://doi.org/10.5194/acp-23-323-2023>, 2023.
- Bilsback, K. R., He, Y., Cappa, C. D., Chang, R. Y.-W., Croft, B., Martin, R. V., Ng, N. L., Seinfeld, J. H., Pierce, J. R., and Jathar, S. H.: Vapors Are Lost to Walls, Not to Particles on the Wall: Artifact-Corrected Parameters from Chamber Experiments and Implications for Global Secondary Organic Aerosol, *Environ Sci Technol*, 57, 53-63, <https://doi.org/10.1021/acs.est.2c03967>, 2023.
- Carlton, A. G., Turpin, B. J., Altieri, K. E., Seitzinger, S. P., Mathur, R., Roselle, S. J., and Weber, R. J.: CMAQ Model Performance Enhanced When In-Cloud Secondary Organic Aerosol is Included: Comparisons of Organic Carbon Predictions with Measurements, *Environmental Science & Technology*, 42, 8798-8802, 10.1021/es01192n, 2008.
- Carlton, A. G., Bhave, P. V., Napelenok, S. L., Edney, E. O., Sarwar, G., Pinder, R. W., Pouliot, G. A., and Houyoux, M.: Model representation of secondary organic aerosol in CMAQv4.7, *Environmental Science & Technology*, 44, 8553-8560, <https://doi.org/10.1021/es100636q>, 2010.
- Chang, X., Zhao, B., Zheng, H., Wang, S., Cai, S., Guo, F., Gui, P., Huang, G., Wu, D., Han, L., Xing, J., Man, H., Hu, R., Liang, C., Xu, Q., Qiu, X., Ding, D., Liu, K., Han, R., Robinson, A. L., and Donahue, N. M.: Full-volatility emission framework corrects missing and underestimated secondary organic aerosol sources, *One Earth*, 5, 403-412, <https://doi.org/10.1016/j.oneear.2022.03.015>, 2022.
- Che, H., Shen, X., Yao, Z., Wu, B., Gou, R., Hao, X., Cao, X., Li, X., Zhang, H., Wang, S., and Chen, Z.: Real-world emission characteristics and inventory of volatile organic compounds originating from construction and agricultural machinery, *Science of The Total Environment*, 894, 164993, <https://doi.org/10.1016/j.scitotenv.2023.164993>, 2023.
- Chen, Q., Miao, R., Geng, G., Shrivastava, M., Dao, X., Xu, B., Sun, J., Zhang, X., Liu, M., Tang, G., Tang, Q., Hu, H., Huang, R.-J., Wang, H., Zheng, Y., Qin, Y., Guo, S., Hu, M., and Zhu, T.: Widespread 2013-2020 decreases and reduction challenges of organic aerosol in China, *Nature Communications*, 15, 4465, <https://doi.org/10.1038/s41467-024-48902-0>, 2024a.
- Chen, W., Hu, W., Tao, Z., Cai, Y., Cai, M., Zhu, M., Ye, Y., Zhou, H., Jiang, H., Li, J., Song, W., Zhou, J., Huang, S., Yuan, B., Shao, M., Feng, Q., Li, Y., Isaacman-VanWertz, G., Stark, H., Day, D. A., Campuzano-Jost, P., Jimenez, J. L., and Wang, X.: Quantitative Characterization of the Volatility Distribution of Organic Aerosols in a Polluted Urban Area: Intercomparison Between Thermodenuder and Molecular Measurements, *Journal of Geophysical Research: Atmospheres*, 129, e2023JD040284, <https://doi.org/10.1029/2023JD040284>, 2024b.
- Chen, W., Ye, Y., Hu, W., Zhou, H., Pan, T., Wang, Y., Song, W., Song, Q., Ye, C., Wang, C., Wang, B., Huang, S., Yuan, B., Zhu, M., Lian, X., Zhang, G., Bi, X., Jiang, F., Liu, J., Canonaco, F., Prevot, A. S. H., Shao, M., and Wang, X.: Real - Time Characterization of Aerosol Compositions, Sources, and Aging Processes in Guangzhou During PRIDE - GBA 2018 Campaign, *Journal of Geophysical Research: Atmospheres*, 126, e2021JD035114, <https://doi.org/10.1029/2021JD035114>, 2021.
- Emery, C. and Tai, E.: Enhanced Meteorological Modeling and Performance Evaluation for Two Texas Ozone Episodes,
- Emery, C., Liu, Z., Russell, A. G., Odman, M. T., Yarwood, G., and Kumar, N.: Recommendations on statistics and benchmarks to assess photochemical model performance, *Journal of the Air & Waste Management Association*, 72, 100-112, <https://doi.org/10.1080/1065248X.2021.1937000>, 2022.

- Management Association (1995), 67, 582-598, <https://doi.org/10.1080/10962247.2016.1265027>, 2017.
- Feng, T., Wang, Y., Hu, W., Zhu, M., Song, W., Chen, W., Sang, Y., Fang, Z., Deng, W., Fang, H., Yu, X., Wu, C., Yuan, B., Huang, S., Shao, M., Huang, X., He, L., Lee, Y. R., Huey, L. G., Canonaco, F., Prevot, A. S. H., and Wang, X.: Impact of aging on the sources, volatility, and viscosity of organic aerosols in Chinese outflows, *Atmospheric Chemistry and Physics*, 23, 611-636, <https://doi.org/10.5194/acp-23-611-2023>, 2023.
- Ge, X., Li, L., Chen, Y., Chen, H., Wu, D., Wang, J., Xie, X., Ge, S., Ye, Z., Xu, J., and Chen, M.: Aerosol characteristics and sources in Yangzhou, China resolved by offline aerosol mass spectrometry and other techniques, *Environmental Pollution*, 225, 74-85, <https://doi.org/10.1016/j.envpol.2017.03.044>, 2017.
- Gu, C., Cui, S., Ge, X., Wang, Z., Chen, M., Qian, Z., Liu, Z., Wang, X., and Zhang, Y.: Chemical composition, sources and optical properties of nitrated aromatic compounds in fine particulate matter during winter foggy days in Nanjing, China, *Environmental Research*, 212, 113255, <https://doi.org/10.1016/j.envres.2022.113255>, 2022.
- Huang, C., Hu, Q., Li, Y., Tian, J., Ma, Y., Zhao, Y., Feng, J., An, J., Qiao, L., Wang, H., Jing, S., Huang, D., Lou, S., Zhou, M., Zhu, S., Tao, S., and Li, L.: Intermediate Volatility Organic Compound Emissions from a Large Cargo Vessel Operated under Real-World Conditions, *Environmental Science & Technology*, 52, 12934-12942, <https://doi.org/10.1021/acs.est.8b04418>, 2018.
- Kohl, I., Bachmann, L., Hallbrucker, A., Mayer, E., and Loerting, T.: Liquid-like relaxation in hyperquenched water at ≤ 140 K, *Physical Chemistry Chemical Physics*, 7, 3210-3220, 2005.
- Li, K., Chen, L., White, S. J., Zheng, X., Lv, B., Lin, C., Bao, Z., Wu, X., Gao, X., Ying, F., Shen, J., Azzi, M., and Cen, K.: Chemical characteristics and sources of PM₁ during the 2016 summer in Hangzhou, *Environmental Pollution*, 232, 42-54, <https://doi.org/10.1016/j.envpol.2017.09.016>, 2018.
- Lu, Q. Y., Murphy, B. N., Qin, M. M., Adams, P., Zhao, Y. L., Pye, H. O. T., Efstathiou, C., Allen, C., and Robinson, A. L.: Simulation of organic aerosol formation during the CalNex study: updated mobile emissions and secondary organic aerosol parameterization for intermediate-volatility organic compounds, *Atmospheric Chemistry and Physics*, 20, 4313-4332, <https://doi.org/10.5194/acp-20-4313-2020>, 2020.
- McDonald, B., de Gouw, J., Gilman, J., Jathar, S., Akherati, A., Cappa, C., Jimenez, J., Lee-Taylor, J., Hayes, P., McKeen, S., Cui, Y., Kim, S.-W., Gentner, D., Isaacman-VanWertz, G., Goldstein, A., Harley, R., Frost, G., Roberts, J., Ryerson, T., and Trainer, M.: Volatile chemical products emerging as largest petrochemical source of urban organic emissions, *Science (New York, N.Y.)*, 359, 760-764, <https://doi.org/10.1126/science.aaq0524>, 2018.
- Murphy, B. N., Woody, M. C., Jimenez, J. L., Carlton, A. M. G., Hayes, P. L., Liu, S., Ng, N. L., Russell, L. M., Setyan, A., Xu, L., Young, J., Zaveri, R. A., Zhang, Q., and Pye, H. O. T.: Semivolatile POA and parameterized total combustion SOA in CMAQv5.2: impacts on source strength and partitioning, *Atmos. Chem. Phys.*, 17, 11107-11133, <https://doi.org/10.5194/acp-17-11107-2017>, 2017.
- Pye, H. O. T., Luecken, D. J., Xu, L., Boyd, C. M., Ng, N. L., Baker, K. R., Ayres, B. R., Bash, J. O., Baumann, K., Carter, W. P. L., Edgerton, E., Fry, J. L., Hutzell, W. T., Schwede, D. B., and Shepson, P. B.: Modeling the Current and Future Roles of Particulate Organic Nitrates in the Southeastern United States, *Environmental Science & Technology*, 49, 14195-14203, <https://doi.org/10.1021/acs.est.5b03738>, 2015.
- Pye, H. O. T., Pinder, R. W., Piletic, I. R., Xie, Y., Capps, S. L., Lin, Y.-H., Surratt, J. D., Zhang, Z., Gold, A., Luecken, D. J., Hutzell, W. T., Jaoui, M., Offenberg, J. H., Kleindienst, T. E., Lewandowski, M., and Edney, E. O.: Epoxide Pathways Improve Model Predictions of Isoprene Markers and Reveal Key Role of Acidity in Aerosol Formation, *Environmental Science & Technology*, 47, 11056-11064,

<https://doi.org/10.1021/es402106h>, 2013.

- Pye, H. O. T., Murphy, B. N., Xu, L., Ng, N. L., Carlton, A. G., Guo, H., Weber, R., Vasilakos, P., Appel, K. W., Budisulistiorini, S. H., Surratt, J. D., Nenes, A., Hu, W., Jimenez, J. L., Isaacman-VanWertz, G., Misztal, P. K., and Goldstein, A. H.: On the implications of aerosol liquid water and phase separation for organic aerosol mass, *Atmos. Chem. Phys.*, 17, 343-369, 10.5194/acp-17-343-2017, 2017.
- Qin, M., Murphy, B. N., Isaacs, K. K., McDonald, B. C., Lu, Q., McKeen, S. A., Koval, L., Robinson, A. L., Efstatiou, C., Allen, C., and Pye, H. O. T.: Criteria pollutant impacts of volatile chemical products informed by near-field modelling, *Nature Sustainability*, 4, 129-137, 2021.
- Shen, X., Che, H., Lv, T., Wu, B., Cao, X., Li, X., Zhang, H., Hao, X., Zhou, Q., and Yao, Z.: Real-world emission characteristics of semivolatile/intermediate-volatility organic compounds originating from nonroad construction machinery in the working process, *Science of The Total Environment*, 858, 159970, <https://doi.org/10.1016/j.scitotenv.2022.159970>, 2023.
- Simon, H. and Bhave, P. V.: Simulating the Degree of Oxidation in Atmospheric Organic Particles, *Environmental Science & Technology*, 46, 331-339, 10.1021/es202361w, 2012.
- Tang, R., Lu, Q., Guo, S., Wang, H., Song, K., Yu, Y., Tan, R., Liu, K., Shen, R., Chen, S., Zeng, L., Jorga, S. D., Zhang, Z., Zhang, W., Shuai, S., and Robinson, A. L.: Measurement report: Distinct emissions and volatility distribution of intermediate-volatility organic compounds from on-road Chinese gasoline vehicles: implication of high secondary organic aerosol formation potential, *Atmospheric Chemistry and Physics*, 21, 2569-2583, <https://doi.org/10.5194/acp-21-2569-2021>, 2021.
- Xian, J., Cui, S., Chen, X., Wang, J., Xiong, Y., Gu, C., Wang, Y., Zhang, Y., Li, H., Wang, J., and Ge, X.: Online chemical characterization of atmospheric fine secondary aerosols and organic nitrates in summer Nanjing, China, *Atmospheric Research*, 290, 106783, <https://doi.org/10.1016/j.atmosres.2023.106783>, 2023.
- Xu, J., Liu, D., Wu, X., Vu, T. V., Zhang, Y., Fu, P., Sun, Y., Xu, W., Zheng, B., Harrison, R. M., and Shi, Z.: Source apportionment of fine organic carbon at an urban site of Beijing using a chemical mass balance model, *Atmospheric Chemistry and Physics*, 21, 7321-7341, <https://doi.org/10.5194/acp-21-7321-2021>, 2021.
- Xu, L., Pye, H. O. T., He, J., Chen, Y., Murphy, B. N., and Ng, N. L.: Experimental and model estimates of the contributions from biogenic monoterpenes and sesquiterpenes to secondary organic aerosol in the southeastern United States, *Atmos. Chem. Phys.*, 18, 12613-12637, <https://doi.org/10.5194/acp-18-12613-2018>, 2018.
- Zhang, Y., Zhang, X., Zhong, J., Sun, J., Shen, X., Zhang, Z., Xu, W., Wang, Y., Liang, L., Liu, Y., Hu, X., He, M., Pang, Y., Zhao, H., Ren, S., and Shi, Z.: On the fossil and non-fossil fuel sources of carbonaceous aerosol with radiocarbon and AMS-PMF methods during winter hazy days in a rural area of North China plain, *Environmental Research*, 208, 112672, <https://doi.org/10.1016/j.envres.2021.112672>, 2022.
- Zhao, B., Wang, S., Donahue, N. M., Chuang, W., Hildebrandt Ruiz, L., Ng, N. L., Wang, Y., and Hao, J.: Evaluation of One-Dimensional and Two-Dimensional Volatility Basis Sets in Simulating the Aging of Secondary Organic Aerosol with Smog-Chamber Experiments, *Environmental Science & Technology*, 49, 2245-2254, <https://doi.org/10.1021/es5048914>, 2015.
- Zhao, J., Qi, L., Lv, Z., Wang, X., Deng, F., Zhang, Z., Luo, Z., Bie, P., He, K., and Liu, H.: An updated comprehensive IVOC emission inventory for mobile sources in China, *Science of The Total Environment*, 851, 158312, <https://doi.org/10.1016/j.scitotenv.2022.158312>, 2022.
- Zhu, W., Zhou, M., Cheng, Z., Yan, N., Huang, C., Qiao, L., Wang, H., Liu, Y., Lou, S., and Guo, S.:

Seasonal variation of aerosol compositions in Shanghai, China: Insights from particle aerosol mass spectrometer observations, Science of The Total Environment, 771, 144948,
<https://doi.org/10.1016/j.scitotenv.2021.144948>, 2021.